Pure & Appl. Chem., Vol. 56, No. 11, pp 1583-1600, 1984.
Printed in Great Britain.

0033-4545/84 $3.00 + 0.00
Pergamon Press Ltd.

NEW TECHNIQUES AND OPPORTUNITIES IN HIGH TEMPERATURE MASS SPECTROMETRY

John W. Hastie

Inorganic Materials Division, National Bureau of Standards, Washington, DC 20234, USA

Abstract - In the present discussion, emphasis is given to recent developments and remaining problems in the application of mass spectrometry to high temperature materials chemistry. Examples of application areas discussed include: Knudsen effusion mass spectrometry of gas-solid reactions, with equilibrium or kinetic control; high-pressure molecular beam sampling mass spectrometry of flames and laser-vapor-plumes, and transpiration mass spectrometry of gas-liquid-solid and ceramic-slag-salt systems. Certain maxims are examined, including use of ionization cross-section approximations. Evidence of departure from the key assumption of a temperature-independent electron impact process is given, including temperature-dependent parent-ion fragmentation and cross section behavior. Errors arising from the use of cross section additivity and electron energy-scaling approximations are also examined.

INTRODUCTION

For the past three decades, high-temperature mass spectrometry has played a key role in the molecular and thermodynamic characterization of high temperature and energy-related materials. Despite the established nature of the field, new developments continue to appear. These modern developments have occurred largely in response to the new challenges of greater accuracy, increasing complexity in chemical systems, more extreme conditions of temperature, pressure, and chemical reactivity, and the need to monitor transient phenomena.

The primary role of high temperature mass spectrometry (HTMS) in defining the chemistry of high temperature and energy-related materials is identification and quantification of vapor and gaseous species. Information concerning the condensed phase follows from thermodynamic cycles and the equivalence of component Gibbs energies at phase boundaries. The unique power of HTMS lies in its ability to analyze complex vapors over a wide molecular weight range (1 to 10^3 amu routinely, to 10^5 amu possible), with a large dynamic range of partial pressure (10^{-14} to > 10 atm) (Note a) and temperature (10 to 5000 K, typically). Furthermore, the vapor can include neutral atomic, molecular, or radical species, as well as ions. These conditions of temperature, pressure and chemical complexity are typical of those found in high-temperature materials applications, such as: combustion (coal, rocket fuels, MHD,...), coal gasification, nuclear fuel meltdown, ceramic processing, chemical vapor deposition, and laser heating. A discussion of the importance of high temperature species in such systems has been given elsewhere (Ref. 1).

Many key developments in measurement science were necessary to the development of HTMS, in its modern form, as shown in Table 1. The listing in Table 1 is representative of the field and emphasizes electron impact mass spectrometry. That is, the more specialized and less routinely used methods of ionization, such as photo- and chemi-ionization (for gaseous organics), are omitted in the present discussion. Berkowitz (22) has reviewed the development and application of photoionization and photoelectron methods for high temperature species. In 1978, a special symposium addressed measurement applications and problems for high-temperature vapors and gases, including HTMS and other complementary methods (Ref. 23). The present discussion deals with some of the more recent developments (identified in Table 1 with an asterisk) using examples from the author's laboratory, and with emphasis on measurement problems in high temperature materials and energy systems.

KNUDSEN EFFUSION MASS SPECTROMETRY (KMS) OF GAS-SOLID (LIQUID) EQUILIBRIA

The KMS method has been the mainstay of HTMS and, indeed, high temperature chemistry in general. However, its usage has been limited primarily to systems with condensible

Note a. 1 atm = 101325 N m^{-2}.

TABLE 1. Some key developments in high temperature mass spectrometry

	Development	Author (Ref.)	Year
1.	Knudsen effusion principle	Knudsen(2)	1909
2.	Electron impact magnetic deflection mass spectrometry of non-volatiles	Dempster(3)	1918
3.	Transpiration method for partial pressures	von Wartenberg et al. (4)	1921
4.	Use of (1) for pressures	Egerton(5)	1923
5.	Flame sampling at low pressure	Eltenton(6)	1947
6.	Vapor species from filament	Ionov(7)	1948
7.	Theory for molecular beam sampling at high pressure	Kantrowitz and Grey (8)	1951
8.	Coupling of (1) and (2)	Chupka and Inghram(9)	1953
* 9.	Additivity of atomic cross sections	Otvos and Stevenson (10)	1956
10.	Quadrupole mass filter	Paul et al (11)	1958
11.	Beam modulation spectroscopy	Fite et al (12)	1964
12.	Extension of (5) to atm flames	Milne and Greene(13)	1965
*13.	Coupling of (1) and (10)	Hastie and Swingler (14)	1966
14.	Calculation of atomic ionization cross sections	Mann(15)	1967
*15.	Extension of (12) to laser vapor plumes	Knox(16)	1968
16.	Sampling of vapor transport	Hager and Hill(17)	1970
*17.	Extension of (12) to condensible inorganic species under kinetic conditions	Hastie(18)	1973
18.	As for (17) but for equilibrated conditions	Farber and Srivastava (19)	1973
*19.	Coupling of (3) and (10)— Transpiration Mass Spectrometry	Bonnell and Hastie (20)	1979
20.	Metal clusters	Sattler et al (21)	1980

(non-scatterable) vapors. Problems associated with the presence of noncondensible gaseous species include: masking of the beam signal by scattered gas of the same molecular weight and, difficulty in achieving gas-solid (liquid) thermodynamic equilibrium. A third problem common in, but not limited to, gas-containing systems includes sample inhomogeneity due to surface segregation by vaporization. Methods used to control these problems include use of shutter profiles of molecular beam intensity distribution, cryogenic surfaces to prevent (reduce) gas scattering, and molecular beam modulation with phase analysis of the ion signal.

Basis of the KMS technique

The beam modulation method has been used extensively in our research and a schematic showing the basic features of the technique is given in Fig. 1. Equation (1) in Fig. 1 is the basic KMS relationship between species partial pressure (P), mass spectral positive ion intensity (I), cell temperature (T), and a system sensitivity factor (k). The k-factor is obtained from a knowledge of ionization cross section (σ) and instrument sensitivity (S), or from a well-established relationship between the time-integrated ion intensity ($\Sigma I\Delta t$), mass loss (Δm), molecular weight (M), and effusion orifice area (A). As discussed elsewhere (Ref. 12), the phase angle difference ($\Delta\phi$) between the ion and wheel reference signals is related to the distance (L) the modulated beam travels prior to ionization, the modulation frequency (f), the molecular weight (M) of the ion precursor and the beam translational temperature (T).

KNUDSEN EFFUSION MASS SPECTROMETRY

(KMS) OF GAS-SOLID (LIQUID) EQUILIBRIA

APPARATUS SCHEMATIC

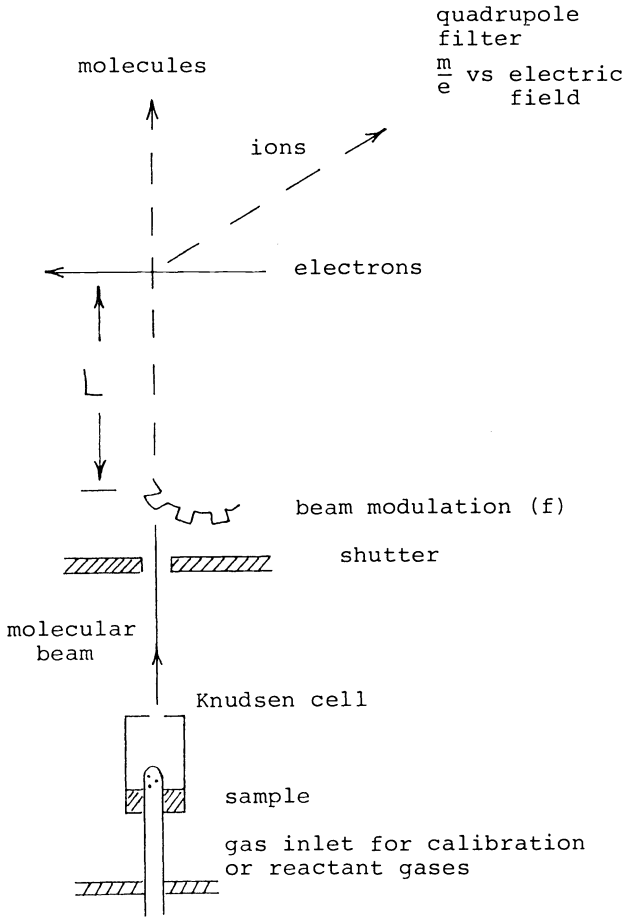

BASIS OF TECHNIQUE

$$P = kIT \quad (1)$$

$$k = f(\sigma, S) \text{ or } (\Sigma I \Delta t, \Delta m, M, A) \quad (2)$$

$$\Delta\Phi = f\left[2\pi f L (M/T)^{1/2}\right] \quad (3)$$

Fig. 1. Schematic of Knudsen effusion mass spectrometric apparatus for analysis of gas-solid (or liquid) equilibria.

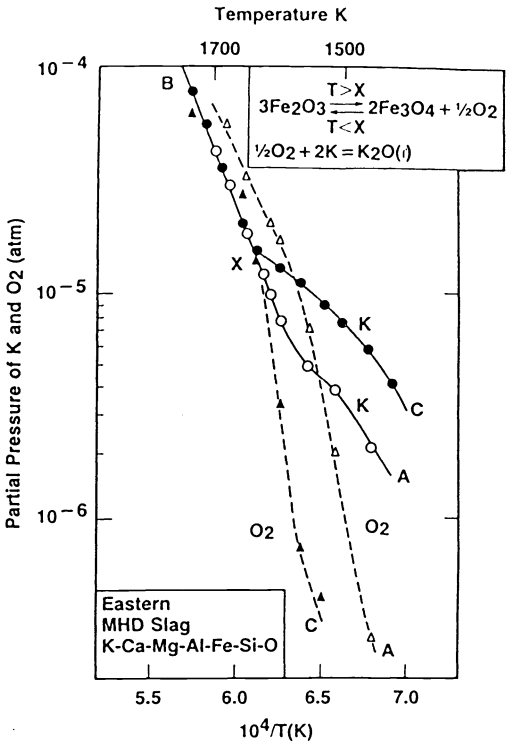

Fig. 2. Vapor pressures over a synthetic magnetohydrodynamic channel Eastern coal slag, enriched with K-seed, and with composition (wt.%) K_2O (23.6), Al_2O_3 (25.5), Fe_2O_3 (12.5), CaO (1.8), MgO (0.6), and SiO_2 (36.0). Run chronology is A-B-C. The solid and dashed curves are for K and O_2 pressures, respectively. From Ref. 24.

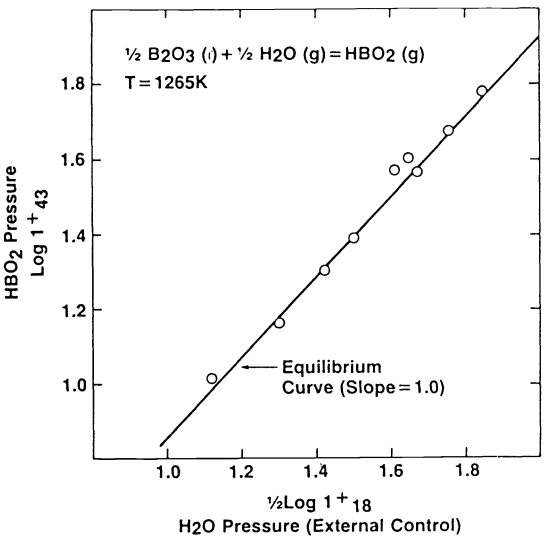

Fig. 3. Test for equilibrium, in the isothermal $B_2O_3(\ell) + H_2O$ system (Ref. 25). Points are experimental data and the curve has slope predicted for equilibrium reaction shown.

Representative data--establishment of equilibrium

An example of a system showing unusual vaporization behavior, resulting from competing equilibria involving a gaseous product (O_2), is given in Fig. 2 (see also Ref. 24). As shown by the reactions listed in the figure, the O_2 and K partial pressures are controlled by the reduction of Fe_2O_3 (at T > X), the oxidation of Fe_3O_4 (at T < X), and also by the temperature dependent thermodynamic activity of $K_2O(\ell)$. Though not readily apparent in the figure, it can be shown that both O_2 and K are in thermodynamic equilibrium with the slag phase. Also, the K_2O activity $[P(K)^2 \cdot P(O_2)^{0.5}]$ follows a single linear curve, as expected, over the temperature interval of Fig. 2.

For cases where the gas pressure can be controlled externally, the Le Chatelier principle of reaction reversibility (or mobile equilibrium) can be used to test for equilibrium, as shown, for example, in Fig. 3. As plotted, the results indicate the presence of equilibrium and establish the reaction stoichiometry given in the figure. The temperature dependence of the equilibrium constant can also be used to test for system equilibrium by comparison of second and third law enthalpies. Figure 4, shows satisfactory agreement with the literature curve for both the slope and intercept and hence the second and third law enthalpies, respectively.

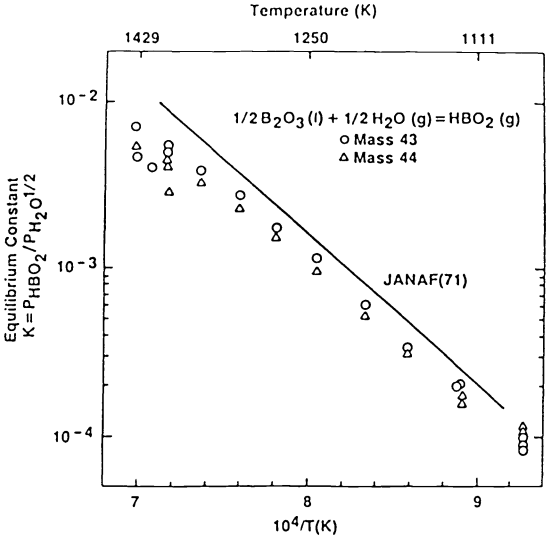

Fig. 4. Test for equilibrium, and comparison with literature data, (solid curve from Ref. 26) for the B_2O_3 (ℓ) + H_2O system (Ref. 25).

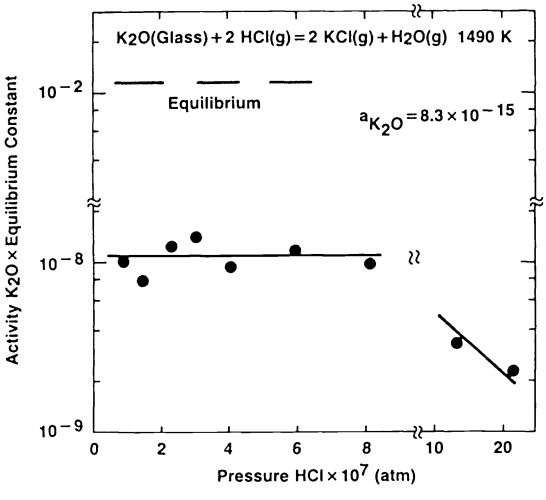

Fig. 5. Test for equilibrium in the K_2O (glass) + HCl system. Glass sample is NBS SRM-621 with composition (wt.%) of Na_2O (12.7), K_2O (2.0), CaO (10.7), MgO (0.27), Al_2O_3 (2.77), and SiO_2 (74.3). The dashed line shows the predicted equilibrium curve (Ref. 27).

Cases where equilibrium is not established

Examples of systems where gas solid (or liquid) equilibrium is not present are given in Figs. 5 and 6. Note in Fig. 5 that the apparent equilibrium constant is insensitive to the HCl pressure at pressures of 1 to 8 x 10^{-7} atm. This observation could be interpreted, erroneously, to indicate an equilibrium condition. Thus the Le Chatelier test for equilibrium can be misleading. These departures from equilibrium are usually less pronounced as the temperature increases, as shown in Fig. 6. In other HCl-oxide studies we have achieved equilibrium with an increase in temperature. Only modest improvements in the approach to equilibrium for these systems was obtained by using the smallest cell orifice area (i.e., gas residence time) possible. As might be expected, higher activity components are more readily equilibrated. For the case of CaO in dolomite (i.e., Fig. 6 system) we observed an equilibrium production of $CaCl_2$ vapor by reaction with HCl. The lack of equilibrium for the example of Fig. 6 is particularly pertinent to the prediction of alkali vapor transport in dolomite-supported fluidized bed coal combustion. In this application, the thermodynamic computer models used may be inappropriate because of the unfavorable gas-solid reaction rate.

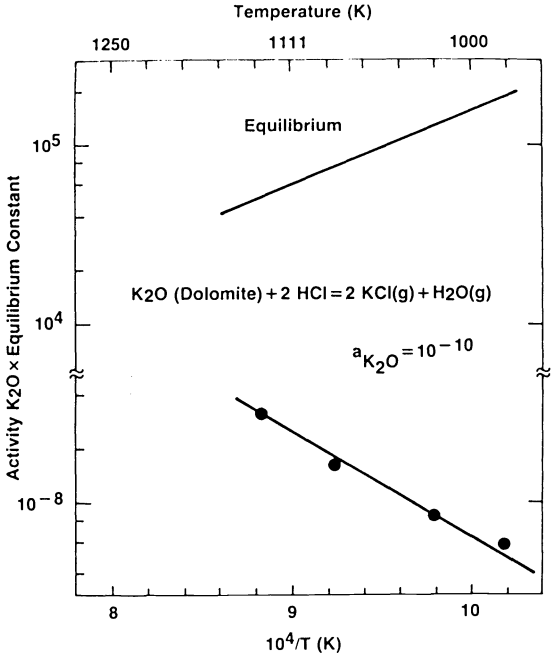

Fig. 6. Test for equilibrium in the K_2O (dolomite) + HCl system, showing a comparison between observed non-equilibrium data (closed circles) and the calculated equilibrium curve. Dolomite sample is NBS SRM-88a with composition (wt.%) of K_2O (0.12), Na_2O (0.01), CaO (30.1), MgO (21.3), Fe_2O_3 (0.28), Al_2O_3 (0.19), SiO_2 (1.20), and CO_2 (46.6). (Ref. 27).

HIGH PRESSURE SAMPLING MASS SPECTROMETRY (HPMS)

For many high temperature systems of practical or scientific interest, the vapor or gas pressures greatly exceed those allowed by the KMS technique ($< 10^{-4}$ atm). The formation of molecular beams from high pressures for mass spectrometric analysis relies on reasonably well established principles of gas dynamics and probe design as discussed in detail elsewhere (e.g. see Ref. 23). An apparatus developed in our laboratory for HPMS is shown schematically in Fig. 7. The representative configuration shown is used for molecular beam sampling from flames at atmospheric pressure. A portion of the flame gas expands through a small knife edged orifice into a vacuum chamber (stage I). The expanding gas jet is skimmed to form a supersonic molecular beam in stage II. This beam is modulated in stage III by a motor driven toothed wheel and mass spectrometrically analyzed in stage IV using a quadrupole filter.

Representative data

The HPMS technique has been particularly useful for obtaining species concentration profiles in flames, from which elementary reaction kinetic descriptions of combustion processes are derived. Figure 8 shows typical concentration profiles for reactant (ϕ_3PO), intermediate (HPO_2), and product (PO) species in a phosphorus-containing flame. These species interact with the flame radicals (H, OH) to inhibit or promote the flame, depending on flame conditions, as discussed in detail elsewhere (Ref. 28). The HPO_2 intermediate is a key species and controls the flame processes via the reaction,

$$HPO_2 + H \rightleftarrows H_2O + PO \quad .$$

In the forward direction, favored at low temperatures, the removal of H atoms leads to flame inhibition. In the backward direction, favored at high temperatures, flame promotion results. Note, in Fig. 8, that HPO_2 greatly exceeds the equilibrium level at the expense of PO. At higher temperatures, and greater distances downstream from the flame reaction zone, these species concentrations approach equilibrium values.

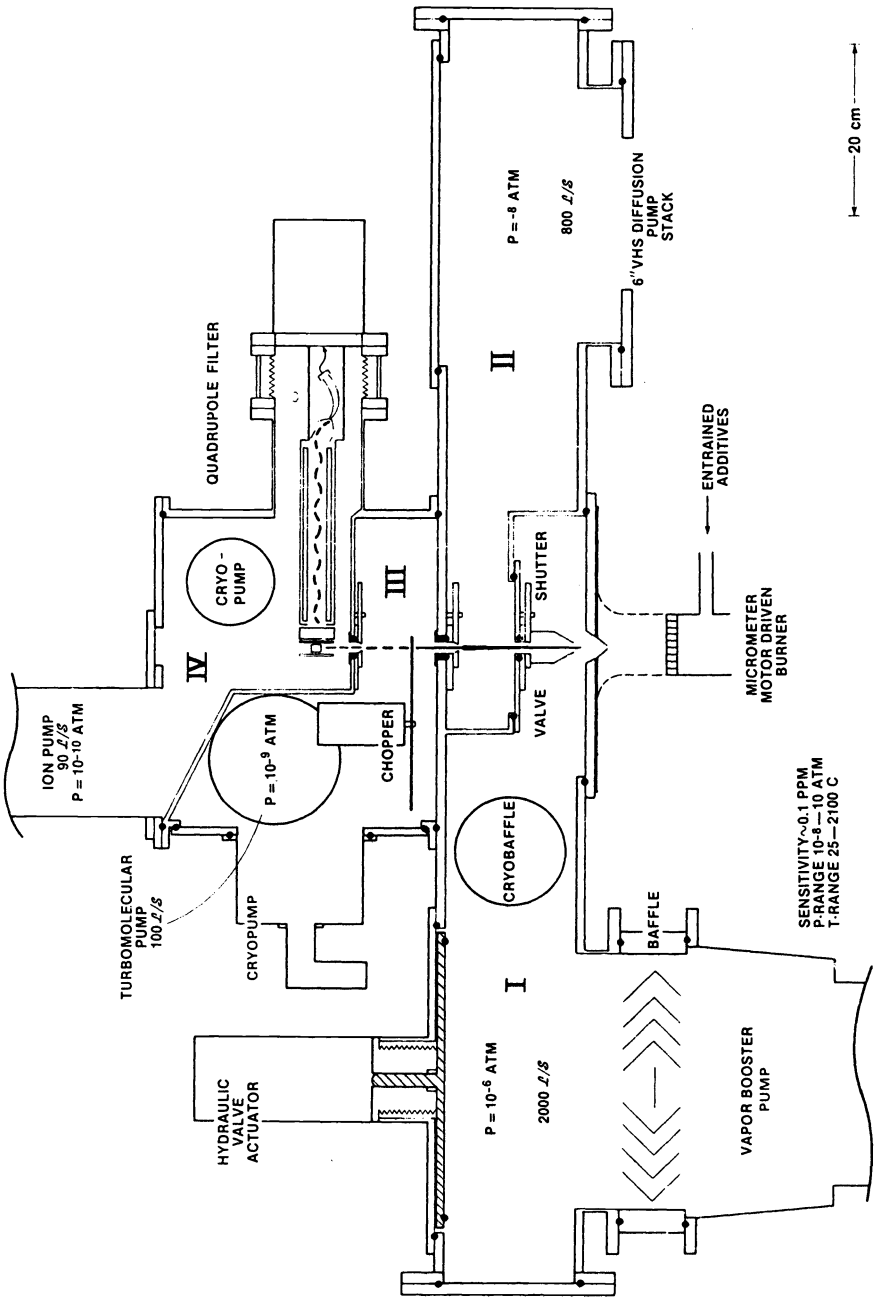

Fig. 7. Scale drawing (ca. one tenth full size) of apparatus for high pressure sampling mass spectrometry, showing flame sampling mode (Ref. 28).

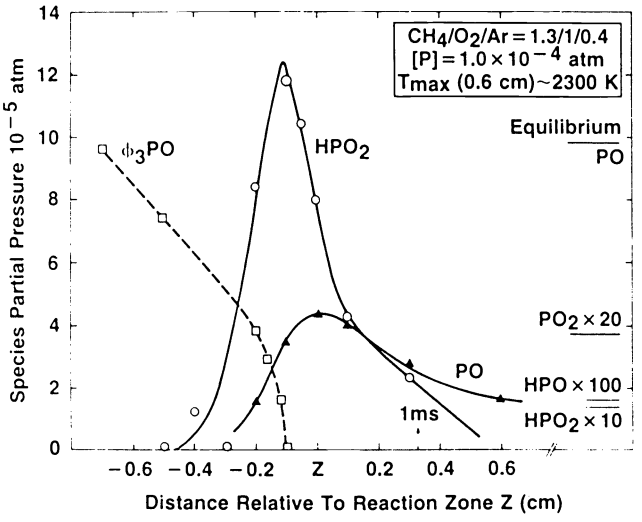

Fig. 8. Species concentration profiles for an atmospheric flame doped with triphenylphosphine oxide. Horizontal bars show calculated equilibrium values (Ref. 28). The flame gases flow from left to right along the distance axis shown.

LASER-INDUCED VAPORIZATION MASS SPECTROMETRY (LIVMS)

Key limitations to high temperature materials chemistry research include the difficulty in achieving high temperatures and the limited availability of non-reactive container materials. Use of focussed laser radiation as a heat source bypasses both of these limitations, and the application of LIVMS has grown rapidly over the past decade; e.g., see Olander (29). Figure 9 shows a schematic of a LIVMS system developed in our laboratory, (Ref. 30). Use of a narrow laser pulse width, a long molecular beam path length, and a signal averager allows time-resolved data to be obtained, as shown in Fig. 10. This time-resolved profile contains information about the beam temperature, molecular thermal distribution, and ion precursor molecular weight. Figure 11 shows the relationship between ion arrival time and precursor molecular weight from which the beam velocity and temperature are derived. This plot also supports the assignment of mass spectral signals to parent ions; that is, interference by electron-impact fragmentation is negligible.

Test for plume-surface equilibrium

Given the Langmuir nature of laser-induced vaporization and the transitory heating process, the presence of thermodynamic equilibrium between the vapor plume and the surface cannot be assumed a priori. The partial pressure ratios for the BN system agree with an equilibrium model where the B/N_2 stoichiometry has been constrained to a mole ratio of 2.0, as shown in Fig. 12 (see Ref. 30).

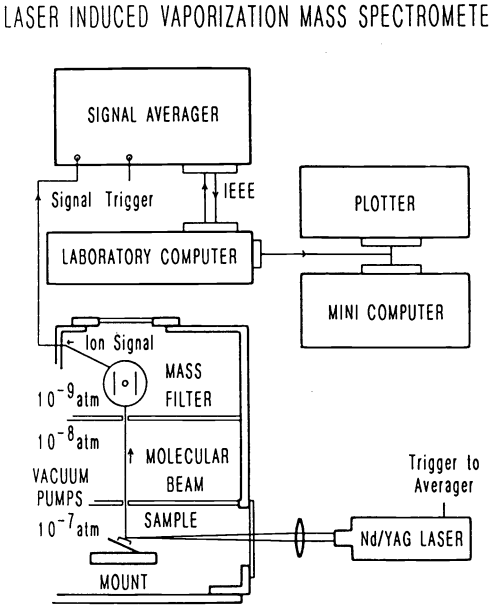

Fig. 9. Schematic of apparatus for laser induced vaporization mass spectrometry (Ref. 30). Details of the vacuum system are given in Fig. 7.

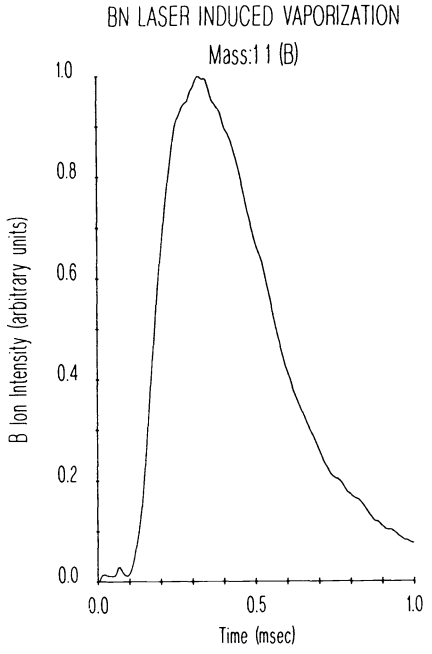

Fig. 10. Time resolved profile of B^+ (B) produced by LIVMS of BN at a surface temperature of 2930 K. The laser on/off condition occurs virtually at the orgin of the time scale indicated.

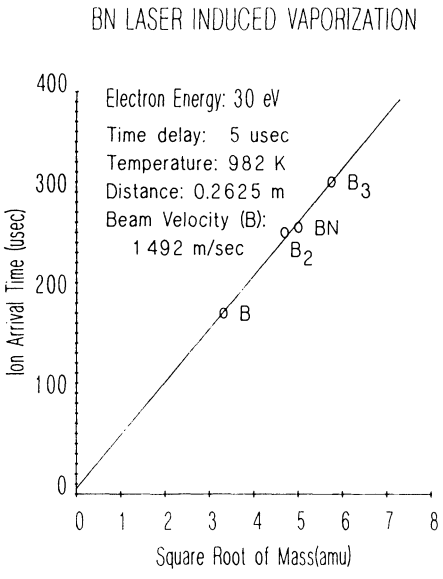

Fig. 11. Species ion-arrival-time dependence on molecular weight produced by LIVMS of BN at 2930 K.

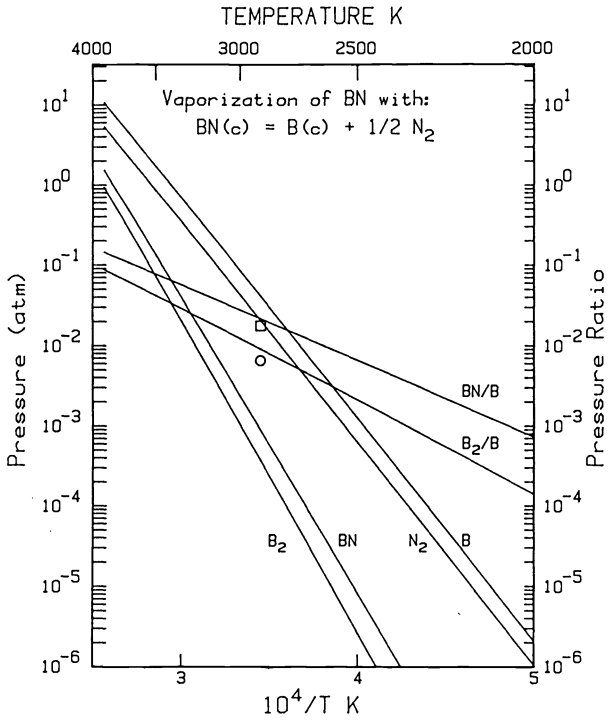

Fig. 12. Test for local equilibrium in the laser induced vaporization of BN. The circle/square data points are the experimental B_2/B and BN/B results, respectively. The curves are from thermodynamic calculations.

TRANSPIRATION MASS SPECTROMETRY (TMS)

Thermodynamic applications

The KMS, HPMS, and LIVMS techniques discussed are not suitable for the analysis of gas-solid (liquid) equilibria at elevated pressures and with predictable temperature control. Transpiration mass spectrometry is particularly well suited to these conditions (Refs. 20, 31). The technique basically couples the classical transpiration and HPMS methods, as shown in Fig. 13. Accurate partial pressure data can be obtained over a wide range of pressure and temperature, as shown in Fig. 14. The technique also extends the temperature and pressure range of the KMS method as shown, for example, in Figs. 15, 16, and 17. The example of Fig. 17 typifies the considerable disagreement that can occur between various researchers and techniques, even for a relatively simple single component system. Only the TMS results are based on direct species-specific measurements over the temperature interval shown. A detailed discussion of this figure has been given elsewhere (Ref. 32).

Cold beam applications

The TMS technique also allows for the controlled cooling of high temperature molecular beams while maintaining the initial species identity and concentration information (see Refs. 20, 31). For a typical source temperature and sampling orifice, the relationship between transport gas pressure and beam temperature is given in Fig. 18. The variables and factors that determine beam temperature (T_b) include: the source temperature (T_o) and pressure (P_o), the nozzle orifice diameter (d), the heat capacity ratio C_p/C_v (γ), a collision diameter factor (σ), and collision effectiveness factor (ε), as discussed in Ref. 31. With the TMS approach, it is possible to vary independently T_o, P_o, d, and γ. As shown in Fig. 18, it is possible to vary T_b over a wide range for convenient changes in P_o.

Temperature-dependent electron-impact ionization. The dramatic cooling effect associated with TMS has been particularly useful in revealing temperature-dependent electron-impact ionization phenomena (Refs. 31 and 33). In the past, high temperature mass spectrometry has relied heavily on the assumption of temperature-independent electron-impact ionization.

For the KCl vapor system, which contains primarily KCl and $(KCl)_2$ species, the electron impact characteristics under hot-beam conditions are well established as discussed in Ref. 32. The K^+ and KCl^+ ions originate from a KCl precursor and K_2Cl^+ is the only significant dimer ion. Thus the ion intensity ratios $R_1 = K^+/KCl^+$ and $R_2 = K_2Cl^+/(K^+ + KCl^+)$ should be constant for fixed sample temperature (T_o). However, on varying the carrier gas pressure and hence the beam temperature (T_b), R_1 changes significantly, as shown in Fig. 19. This effect is attributed to temperature-dependent electron impact ionization and results from a changing Franck-Condon efficiency with changing populations of vibrational/rotational states in KCl. A similar behavior is found with the NaCl system, as shown in Fig. 20.

The model curves of Fig. 20 were derived from the potential energy model depicted in Fig. 21. Basically, the values of R at various T_b are related to the summation of vibrational eigen functions on either side of a critical distance r_c, where stable $NaCl^+$ (or KCl^+) ions result only from transitions where $r > r_c$. The population of each vibrational level is taken as the Boltzman distribution value at T_b. One can see from Fig. 21 that the qualitative effect of an increased temperature (higher v-level population) is to increase the probability that vertical ionization transitions intersect the MX^+ potential curve below the dissociation limit (to $M^+ + X$). Thus R_1 is predicted to decrease with increased temperature, as observed. Note (in Fig. 20) that the difference between the model and effusive data can be attributed to the approximation of using harmonic oscillator functions in an anharmonic potential well.

At beam temperatures typical of KMS, the R_1 ratio is effectively temperature insensitive e.g., see Fig. 20. Thus KMS experiments do not readily reveal evidence of temperature-dependent electron impact ionization. However, the As_4O_6 system has been interpreted to show such behavior in KMS experiments (Ref. 34). Alternative chemical explanations are also possible (Ref. 35). Using the TMS technique (Ref. 36) we find no evidence of the temperature-dependent ionization suggested by the KMS experiments of Drowart (34); e.g., see Fig. 22. For the conditions depicted in Fig. 22, As_4O_6 is the sole molecular species present and the major ions are $As_4O_6^+$ and $As_3O_4^+$ at 20 eV ionizing electron energy. The "true curve" is in reason-

TRANSPIRATON MASS SPECTROMETRY (TMS)

APPARATUS SCHEMATIC

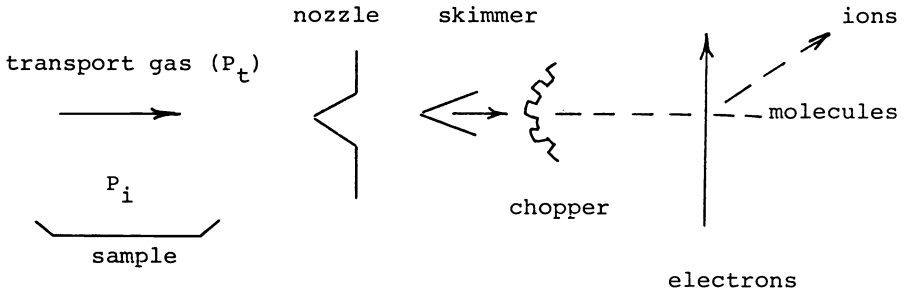

BASIS OF TECHNIQUE

In Transpiration Region

$$\frac{P_i}{P_i + P_t} = \frac{n_i}{n_i + n_t}$$

In Mass Spectrometer

$$P_i = k_i I_i T$$

$$k_i = f(n_i, n_t) = f(\sigma_i, \sigma_t, S_t)$$

Fig. 13. Schematic of transpiration mass spectrometric apparatus with the basic equations also indicated (Ref. 20). The n terms represent moles of species (i) or transport gas (t) transported as determined gravimetrically and volumetrically, respectively. All other terms have been defined elsewhere in the discussion of Knudsen effusion mass spectrometry.

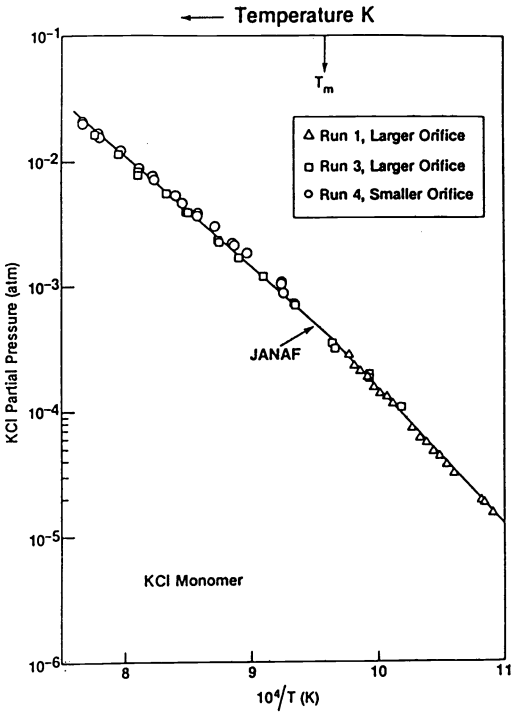

Fig. 14. Comparison of experimental TMS (data points) and literature (solid curve, JANAF, Ref. 26) KCl partial pressures obtained over solid and liquid KCl (Ref. 32).

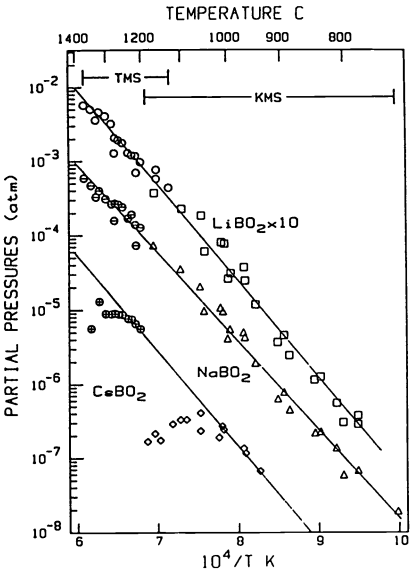

Fig. 15. Comparison of TMS and KMS alkali metaborate partial pressures over a simulated nuclear waste glass with composition (wt. %), SiO_2 (53.8), Fe_2O_3 (11.5), Al_2O_3 (4.8), B_2O_3 (6.5), Li_2O (4.0), Na_2O (8.6), MnO_2 (3.6), NiO (1.8), CaO (1.0), MgO (0.5), ZrO_2 (3.8), SrO (0.05), Cs_2O (0.07), RuO_2 (0.11), and Re_2O_7 (0.03). (Ref. 25).

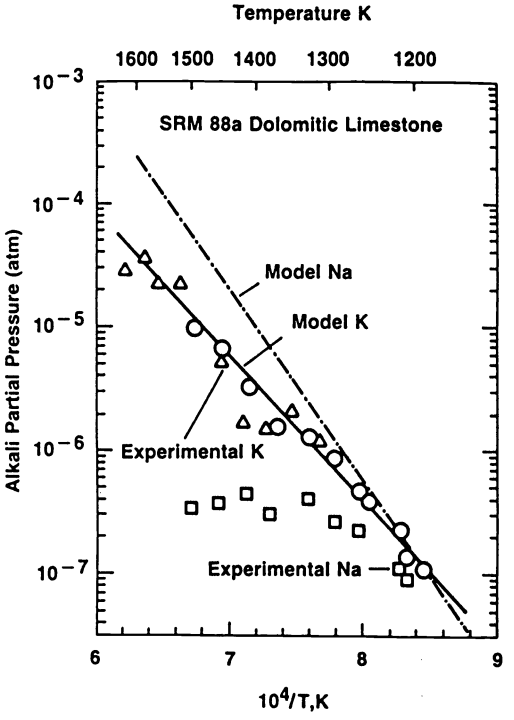

Fig. 16. Comparison of model and experimental alkali partial pressure data for dolomitic limestone (see Fig. 6 caption for composition), showing good agreement between a thermodynamic solution model and experiment and also between the two independent measurement techniques of transpiration (triangular points) and Knudsen effusion (circle and square points) mass spectrometry. The solid and broken curves represent the model predictions of the K and Na pressures, respectively (Ref. 31).

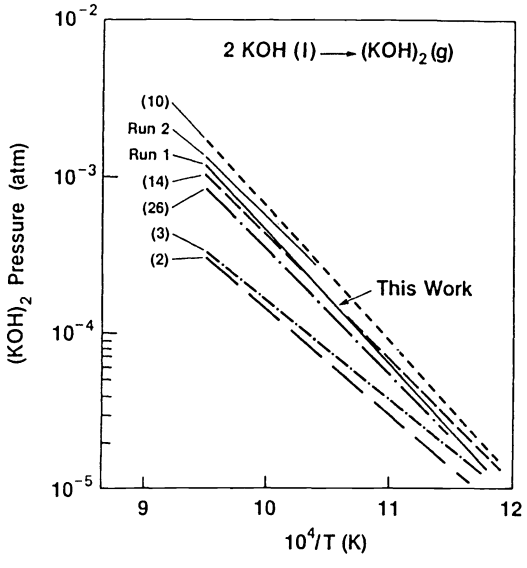

Fig. 17

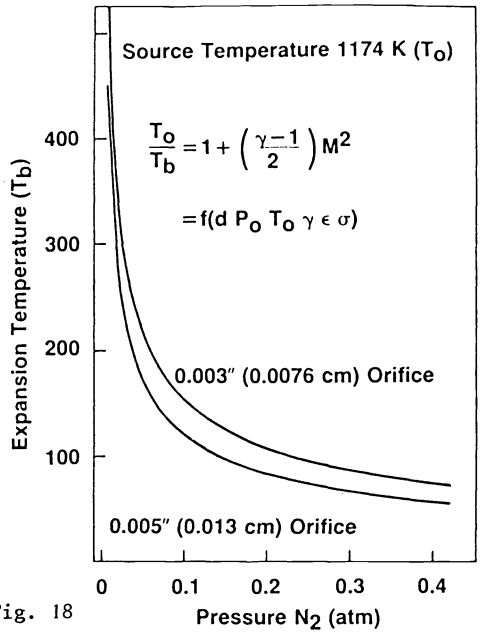

Fig. 18

Fig. 17. Comparison of $(KOH)_2$ partial pressure data (Runs 1 and 2) with literature results, showing the wide disparity among workers. See Ref. 32 for details, including literature citations.

Fig. 18. Calculated dependence of expansion (beam) temperature on source pressure and orifice diameter (Ref. 32).

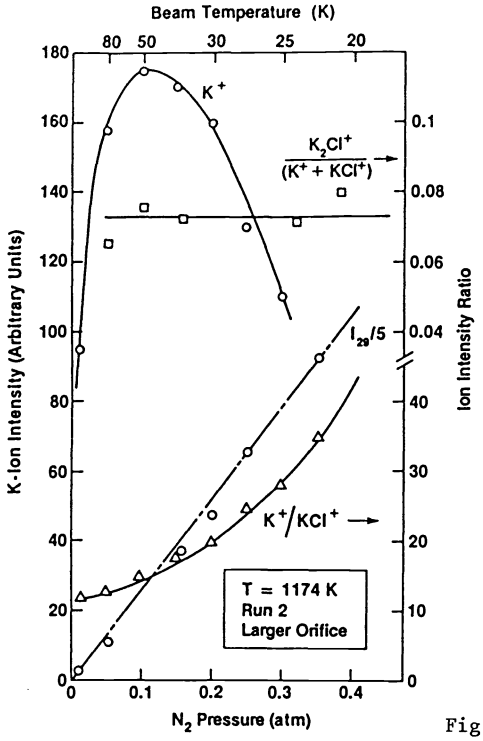

Fig. 19

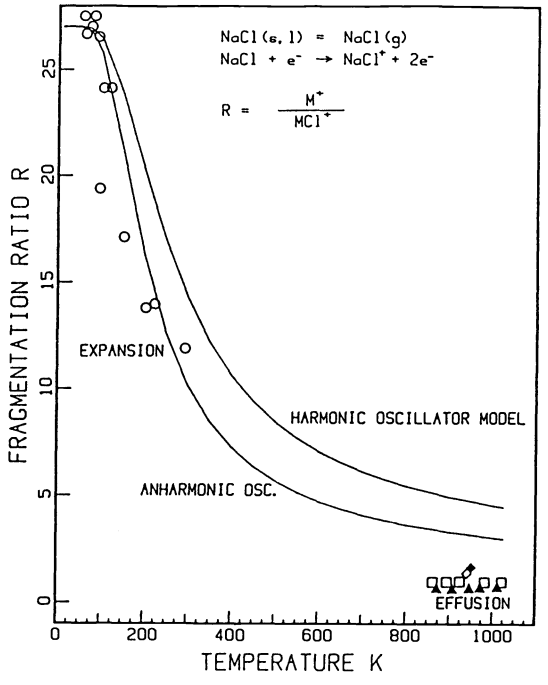

Fig. 20

Fig. 19. Dependence of ion intensities and ratios on source pressure for the KCl system (Ref. 32). The I_{29} curve represents the N_2 carrier gas ion intensity behavior, using the $N^{14}N^{15}$ isotopic signal.

Fig. 20. Comparison of experimental (data points) and model (solid curves) $Na^+/NaCl^+$ ion intensity ratios as a function of beam temperature (Ref. 33). The circle points represent TMS data and the high temperature data points are from KMS experiments made in this and other laboratories.

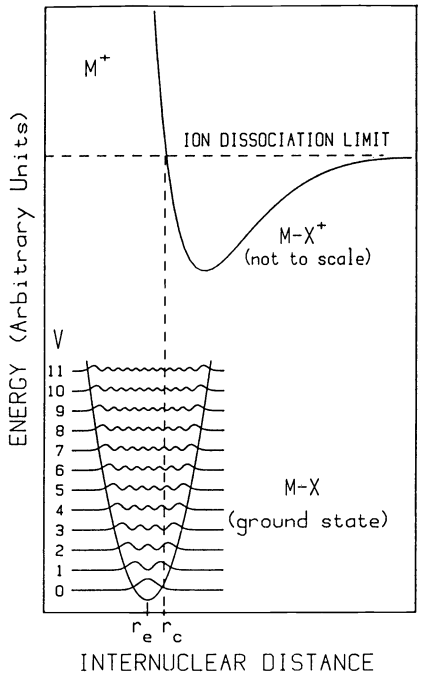

Fig. 21. Potential energy model for alkali halide temperature-dependent electron impact fragmentation, showing details of the square of the oscillator eigenfunctions (Ref. 33).

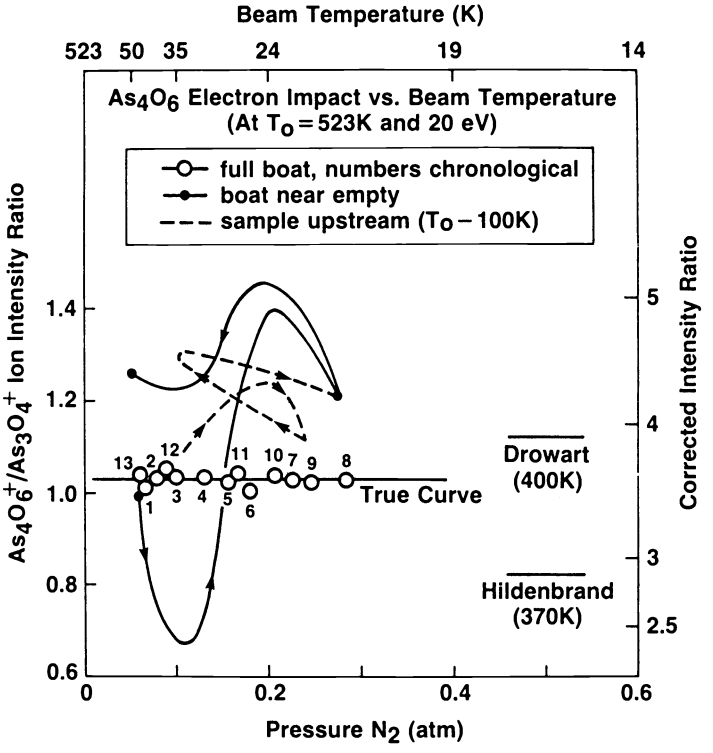

Fig. 22. Dependence of ion intensity ratios on source pressure/beam temperature for the As_4O_6 system (Ref. 36). The data points for the "true curve" are numbered chronologically; the other two curves are examples for nonequilibrium conditions and are not pertinent to the present discussion.

able agreement with the low temperature literature data of Drowart (34) and Hildenbrand (35), but not with their higher temperature data (not shown in Fig. 22).

Based on the limited evidence obtained to date for temperature-dependent electron-impact ionization of high-temperature species, one can rationalize the effect as follows. From a knowledge of ionization potentials and molecular species bond dissociation energies, the relative stability of molecular ion and precursor bonds can be calculated (e.g. see Ref. 37). Where large changes in bond stability occur on ionization, one can expect the location and shape of the molecular-ion potential energy surface to differ considerably from that for the neutral precursor. The example shown in Fig. 21 represents this situation; i.e., $D(M\text{-}X) >> D(M\text{-}X)^+$. It follows that the Franck-Condon transitions will be particularly sensitive to the vibrational-rotational state population distribution, and hence the temperature. Thus, for the alkali halides R_1 is particularly temperature sensitive. However, for the As_4O_6 system, we can show that the stabilities of $As_4O_6^+$ and As_4O_6 are comparable and Franck-Condon transitions should be predominately to a stable region of the $As_4O_6^+$ potential energy surface. Molecular orbital arguments, together with Koopman's principle for ionization, can be used to assess the likelihood of temperature-dependent ionization in other high temperature species (see Ref. 38).

Ionization cross section measurement

In HTMS, two basic methods are used for ionization cross section measurement, as summarized in Table 2. Both methods rely on ion intensity comparisons with species (j) of known ionization cross section, e.g., Ag or N_2. Then, the cross section for species (i) is given by the relationship:

$$\sigma_i = (P_j \cdot \sigma_j \cdot S_j)(P_i \cdot I_j)^{-1}[\sum(I_i/S_i)].$$

The last term is summed over all ions resulting from the precursor (i). Hence a knowledge of the parent ion fragmentation to yield daughter ions is necessary to obtain total ionization cross sections.

TABLE 2. Ionization cross section measurement[a]

1. Integrated Ion Intensity - Gravimetric Methods

   - measure $I\Delta t$ and Δm relative to calibrant
   - calibrate k with material of known P and σ (e.g., Ag or N_2)
   - used with KMS and TMS methods where P unknown
   - for multicomponents, no calibrant needed for a relative σ measurement

2. Manometric - TMS Method

   - $k_j = P_j \cdot (I_j T)^{-1}$
   - use gas reference with known σ_j and manometric P_j
   - use $k_i = P_i \cdot (I_i T)^{-1}$ for known P_i
   - or $k_i = R \cdot (n/V)(\Delta t/\Sigma I \Delta t)$ for P_i unknown
   - then $\sigma_i = \sigma_j \cdot (k_j/k_i)(S_j/S_i)$

[a]Notation not defined in previous discussion: i and j are different species identities, R the Universal gas constant, n moles of i, V volume of j; the S terms are sensitivity calibration factors for molecular weight-dependent effects of Mach focussing, quadrupole filter mass discrimination, and multiplier efficiency.

A number of workers have used the integrated ion intensity-gravimetric method, e.g., see Stafford (39) and Sheldon and Gilles (40). However, studies of this type are relatively few and molecular ionization cross sections are usually estimated. With the TMS method, an additional approach using manometric data can be used, as indicated in Table 2. Cross section values obtained by this method are summarized in Table 3, together with values estimated by the additivity-of-atomic-cross-sections method. Note that on the average the widely used additivity method overestimates cross sections by about a factor of two. However, for the most polyatomic case of As_4O_6 the additivity approach underestimates σ by a factor of two. The inadequacy of this additivity approximation has long been recognized, e.g., see the early review of Drowart (42). However, researchers are still required to rely on this procedure owing to the lack of experimental cross section data (e.g., see Kingcade et al., Ref. 43).

TABLE 3. Cross section (σ) values obtained by TMS at 30 eV (units πa_o^2)[a]

Species	Observed(O)[b]	Additivity(A)[c]	O/A
Ar	2.6 (reference)[a]	-	-
N_2	1.48 (1.2)[a]	2.54	0.58
O_2	1.26 (1.12)[a]	2.41	0.52
H_2	0.76 (0.78)[a]	0.43	1.77
HCl	2.3	3.32	0.69
SO_2	1.3	6.17	0.21
H_2O	1.5	1.63	0.92
Na	4.6 (3.92)[c]	-	-
NaCl	1.0	7.03	0.14
KCl	7.4	10.15	0.73
CsCl	3.1	13.63	0.23
$(KCl)_2$	5.5	20.30	0.27
KOH	2.7	8.47	0.32
$(KOH)_2$	3.6	16.93	0.21
As_4O_6	54.	25.12	2.15
			Average = 0.67

[a] See review of Kieffer and Dunn (41).
[b] Typical uncertainty ± 0.2.
[c] See Mann (15); his Table III maximum cross-sections have been renormalized to the observed reference value in this table.

As was noted in the previous section, electron impact fragmentation can be temperature dependent. Total ionization cross sections are universally assumed to be temperature insensitive. However, as can be seen in Fig. 19 the K^+ ion, which approximately represents the total ionization of KCl, varies in relative intensity with respect to $I(N_2)/P(N_2)$. This varying $I(K^+)\cdot P(N_2)/I(N_2)$ term also indicates that $\sigma(KCl)/\sigma(N_2)$ varies with T_b.

Another maxim of high temperature mass spectrometry involves the following scaling behavior for <u>total</u> ionization cross sections. For an ionizing electron energy E < E(max), where E(max) is the energy (typically 50 to 100 eV) corresponding to the maximum cross section σ(max), the cross section at E is given by:

$$\sigma(E) = \sigma(max)\cdot(E-A)\,[E(max)-A]^{-1} ,$$

where A is the appearance (ionization) potential for the molecular ion. This relationship follows from the proportionality of σ and I and an idealized linear appearance potential curve over the energy interval A to E(max). For the case of practical interest, where partial pressure ratios (of species 1 and 2) are determined from ion intensities (I_1 and I_2) measured at E, the σ - scaling relationship gives:

$$\frac{\sigma_2(E)}{\sigma_1(E)} = \frac{\sigma_2(max)(E-A_2)\,[E_1(max)-A_1]}{\sigma_1(max)(E-A_1)\,[E_2(max)-A_2]}$$

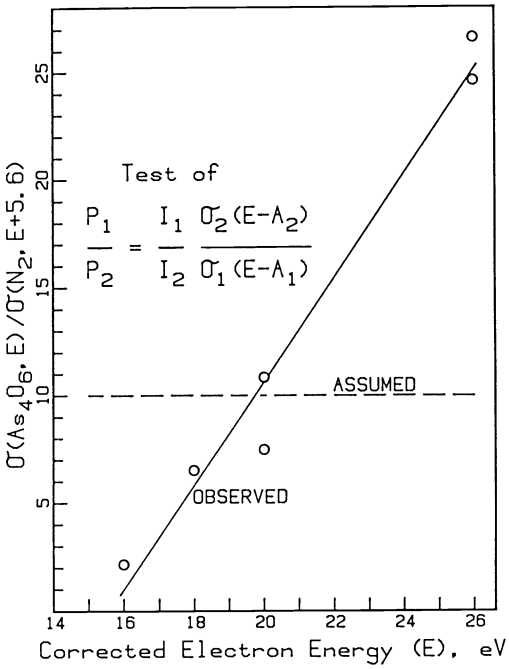

Fig. 23. Variation of total ionization cross section ratios for As_4O_6 and N_2 with electron energy. The cross-sections were obtained at the same energy interval above the appearance potentials of the respective species (10.0 and 15.6 eV for As_4O_6 and N_2, respectively). The N_2 data are from Ref. 41 and the As_4O_6 results were obtained by TMS (Ref. 36).

In past practice the square bracketted terms have been neglected. This approximation basically assumes a constant energy interval between the appearance potential and the energy of maximum cross-section for all species. However, since E(max) is known to vary over a much wider range than A for high temperature species, this is not always a good approximation. These relationships and assumptions provide the basis for the following expression which is in widespread use for the measurement of relative partial pressures:

$$\frac{P_1}{P_2} = \frac{\sigma_2 I_1 (E-A_2)}{\sigma_1 I_2 (E-A_1)} \quad ,$$

where the σ's are maximum cross-sections and the I's are determined at energy E, e.g., see Drowart et al. (44). The validity of this expression for high temperature species has not been stringently tested but scattered observations suggest significant errors can result from its use. Figure 23 shows a serious failure of the underlying cross-section scaling assumptions for the case of As_4O_6. The "assumed" curve is based on the standard practice of estimating molecular cross sections from the atomic data of Mann (15), together with the σ - scaling approximations.

REMAINING PROBLEMS AND FUTURE PROSPECTS

Problem areas requiring much additional work, in addition to several avenues for fruitful future research, are suggested as follows. First, the perennial problem of unknown ionization cross sections remains unresolved for high temperature molecular species. In addition, it now appears that cross-section approximations in current use are not as reliable as expected. Possible variations of total and partial ionization cross-sections with temperature cannot be neglected. Development of an urgently needed theoretical basis for molecular ionization cross sections, coupled with systematic experimental meaurements, could alleviate many of these problems.

The development of high-pressure sampling techniques, with resultant high-intensity, low temperature molecular beams, provides us with an opportunity to couple mass spectrometry with optical spectroscopic, microwave, and other speciation methods. Many of the structural uncertainties arising from the spectroscopic complexity of hot species, together with species assignment problems, could be resolved by this approach.

An opportunity, and need, exists for an expanded effort in the measurement of partial pressure and activity data for high-temperature and refractory systems. Recent successes in thermodynamic solution modeling for alloy (e.g., Ref. 45) and ceramic (e.g., Ref. 46) systems provides an additional impetus for such experiments.

Developments in the controlled production of inorganic cluster species, coupled with mass spectrometric analysis, provides a unique opportunity to bridge our understanding of the vapor and condensed states (Ref. 47). Such an activity could lead to replacement of the classical theory of homogeneous nucleation with a much needed molecular theory. Production of novel materials, by deposition of cluster species with controlled properties, is also an exciting prospect.

Acknowledgments

It is a pleasure to acknowledge that much of the research leading to the developments and examples considered in this overview was carried out in collaboration with my NBS colleagues, Dr. David W. Bonnell, Dr. Ernest R. Plante, Dr. Peter K. Schenck, and Mr. Arthur B. Sessoms, and also with Dr. Kiro F. Zmbov (NBS guest worker) of the Boris Kidrich Institute, Yugoslavia. Contract support on various aspects of high temperature mass spectrometry has been provided by the Department of Energy, Army Research Office, Air Force Office of Scientific Research and the Defense Nuclear Agency.

REFERENCES

1. J.W. Hastie, High Temperature Vapors-Science and Technology, Academic Press, New York (1975).
2. M. Knudsen, Ann. Physik 28, 75 (1909).
3. A.J. Dempster, Phys. Rev. 11, 316 (1918).
4. H. von Wartenberg and P. Albrecht, Z. Elektrochem. 27, 162 (1921).
5. A.C. Egerton, Proc. Roy. Soc. 103A, 469 (1923).
6. G.C. Eltenton, J. Chem. Phys. 15, 455 (1947).
7. N.I. Ionov, Dokl. Akad. Nauk SSSR 59, 467 (1948).
8. A. Kantrowitz and J. Grey, Rev. Sci. Instr. 22, 328 (1951).
9. W.A. Chupka and M.G. Inghram, J. Chem. Phys. 21. 371 (1953).
10. J.W. Otvos and D.P. Stevenson, J. Amer. Chem. Soc. 78, 546 (1956).
11. W. Paul, H.P. Reinhard, and U. von Zahn, Z. Physik 152, 143 (1958).
12. H. Harrison, D.G. Hummer and W.L. Fite, J. Chem. Phys. 41, 2567 (1964).
13. T.A. Milne and F.T. Greene, Tenth Symp. (Int.) Combust. p. 153. The Combustion Institute (1965).
14. J.W. Hastie and D. Swingler, High Temp. Science 1, 46 (1969); J.W. Hastie, Molten Salts and Their Vapours, Ph.D. Thesis, University of Tasmania (1966).
15. J.B. Mann, J. Chem. Phys. 46, 1646 (1967).
16. B.E. Knox, Mat. Res. Bull. 3, 329 (1968).
17. J.P. Hager and R.B. Hill, Metall. Trans. 1, 2723 (1970).
18. J.W. Hastie, Combust. Flame 21, 49 (1973).
19. M. Farber and R.D. Srivastava, Combust. Flame 20. 33 (1973).
20. D.W. Bonnell and J.W. Hastie, Transpiration Mass Spectrometry of High Temperature Vapors, p. 357, in Characterization of High Temperature Vapors and Gases, J.W. Hastie, ed., NBS SP 561/1 and 2, U.S. Govt. Printing Office, Washington, DC (1979).
21. K. Sattler, J. Muhlbach, E. Recknagel, and A. Reyes Flotte, J. Phys. E13, 673 (1980).
22. J. Berkowitz, Photoionization Mass Spectrometry and Photoelectron Spectroscopy of High Temperature Vapors, p. 123 in Advances in High Temperature Chemistry, Vol. 3, L. Eyring, ed., Academic Press, NY (1971).
23. J.W. Hastie, ed., Characterization of High Temperature Vapors and Gases, NBS SP 561/1 and 2, U.S. Govt. Printing Office, Washington, DC (1979). Proc. Tenth Materials Research Symp., Gaithersburg, MD, Sept. 18 (1978).
24. J.W. Hastie and E.R. Plante, Mass Spectrometric Studies of MHD Slag Thermochemistry, NBSIR 81-2293 (1981).
25. J.W. Hastie, E.R. Plante, and D.W. Bonnell, Vaporization of Simulated Nuclear Waste Glass, NBSIR 83-2731 (1983).
26. JANAF Thermochemical Tables, Second Ed., D. R. Stull, and H. Prophet, NSRDS-NBS 37, U.S. Govt. Printing Office, Washington, DC (1971).
27. E.R. Plante, J.W. Hastie, and D.W. Bonnell, Studies of Halogen-Alkali Silicate Interactions, 31st Ann. Meeting Amer. Soc. Mass. Spec., Boston (1983).
28. J.W. Hastie and D.W. Bonnell, Molecular Chemistry of Inhibited Combustion Systems, NBSIR 80-2169 (1980).
29. R.A. Olstad and D.R. Olander, J. Appl. Phys. 46. 1499 (1975).
30. J.W. Hastie, P.K. Schenck, D.W. Bonnell, and E.R. Plante, Characterization of Microwave Window Materials --Molecular Level Vaporization Studies, NBS Final Report to DNA, Nov. (1983).
31. J.W. Hastie and D.W. Bonnell, Transpiration Mass Spectrometry --A New Thermochemical Tool, in "Thermochemistry Today and Its Role in the Immediate Future," M.A. Ribeiro da Silva, ed., Reidel Publ., Boston (1983). In Press.
32. J.W. Hastie, K.F. Zmbov, and D.W. Bonnell, Transpiration Mass Spectrometric Analysis of Liquid KCl and KOH Vaporization, High Temp. Science (1983). In Press.

33. D.W. Bonnell and J.W. Hastie, A Theoretical Analysis of Temperature Dependent Electron Impact Fragmentation, 31st Ann. Meeting Amer. Soc. Mass Spec., Boston (1983).
34. J. Drowart, Thermodynamic Studies at High Temperatures by the Mass Spectrometric Knudsen Cell Method, 29th Ann. Conf. Mass Spec. and Allied Topics, May 24-29 (1982).
35. R.D. Brittain, K.H. Lau, and D.L. Hildenbrand, J. Phys. Chem. 86, 5072 (1982).
36. J.W. Hastie, D.W. Bonnell, and K. F. Zmbov, Transpiration Mass Spectrometric Analysis of the As_4O_6 System. To be published (1984).
37. J.W. Hastie and J.L. Margrave, Fluorine Chem. Rev. 2, 77 (1968).
38. J.W. Hastie and J.L. Margrave, High Temp. Science 1, 481 (1969).
39. J.L. Cooper, Jr., G.A. Pressley, Jr., and F.E. Stafford, J. Chem. Phys. 44. 3946 (1966).
40. R.I. Sheldon and P.W. Gilles, p. 231 in Ref. 23.
41. L.J. Kieffer and G.H. Dunn, Rev. Mod. Phys. 38, 1 (1966).
42. J. Drowart, "Mass Spectrometric Studies of the Vaporization of Inorganic Substances at High Temperatures," p. 255-310, in Int. Symp. on Condensation and Evaporation of Solids, ed., E. Rutner, P. Goldfinger, and J. P. Hirth; Gordon and Breach (1964).
43. J.E. Kingcade, D.L. Cocke, and K.A. Gingerich, High Temp. Science 16, 89 (1983).
44. J. Drowart, G. DeMaria, and M.G. Inghram, J. Chem. Phys. 29, 1015 (1958).
45. K.C. Hsieh, M.S. Wei, and Y. Austin Chang, Z. Metallkd, 74, 330 (1983).
46. J.W. Hastie, D.W. Bonnell, E.R. Plante, and W.S. Horton, "Thermodynamic Activity and Vapor Pressure Models for Silicate Systems, Including Coal Slags," in Thermochemistry Today and Its Role in the Immediate Future, M.A. Ribeiro da Silva, Ed., Reidel Publ., Boston, MA (1983).
47. A.W. Castleman, Jr., "Introduction: Advances and Opportunities in Cluster Research," XIII Int. Conf. Physics of Electronic and Atomic Collisions, Berlin, July 27-August 2, 1983. Eds. J. Eichler, I.V. Hertel, and N. Stollerfoht, North-Holland, New York, NY (1983).